Processing and Application of Ceramics 11 [4] (2017) 275–281
https://doi.org/10.2298/PAC1704275A

Effect of Zr addition on structure and electrical properties of $SmFeO_3$ prepared by solid state reaction method

Abdalla M. Abdalla[1,2,*], Shahzad Hossain[1,3,*], Pg. Mohd. I. Petra[1], Abul K. Azad[1,*]

[1]*Faculty of Integrated Technologies, University Brunei Darussalam, Jalan Tungku Link, Gadong BE1410, Brunei Darussalam*
[2]*Mechanical Engineering Department, Faculty of Engineering, Suez Canal University, Ismailia 41522, Egypt*
[3]*Institute of Nuclear Science and Technology, Bangladesh Atomic Energy Commission, GPO Box No. 3787, Dhaka 1000, Bangladesh*

Received 27 April 2017; Received in revised form 1 August 2017; Received in revised form 12 October 2017; Accepted 15 November 2017

Abstract

Series of $Sm_{1-x}Fe_{1-3x}Zr_{3x}O_3$ (SFZO, where x = 0.0, 0.01, 0.02, 0.033, 0.05, 0.1 and 0.15), was synthesised by the solid state reaction method and sintered at 1500 °C in air. X-ray diffraction (XRD) and scanning electron microscopy (SEM) were used to investigate the structure of the materials. The XRD results indicated that the pure $SmFeO_3$ and $Sm_{0.99}Fe_{0.97}Zr_{0.03}O_3$ samples are single phase materials with an orthorhombic symmetry and Pbnm space group. The increase of Zr content ($x \geq 0.02$) causes a phase change from single to two-phase system with orthorhombic (Pbnm) and fluorite symmetry ($Fm\bar{3}m$). The microstructural analyses showed that the Zr^{4+} doping resulted in an increase of porosity in the sintered SFZO compared to $SmFeO_3$ sample. The direct current (DC) electrical conductivity at 850 °C in air was found to be 0.045 S/cm and 0.007 S/cm for $Sm_{0.99}Fe_{0.97}Zr_{0.03}O_3$ and $SmFeO_3$, respectively, showing a significant enhancement compared to the pure $SmFeO_3$.

Keywords: *perovskite, solid state reaction, structural morphology, electrical conductivity*

I. Introduction

The material properties might be improved by substitution or doping. This is basically related to the atomic arrangement in the material structure [1,2]. This development is important for the design of new materials and provides essential features for various applications, specifically in gas sensors and solid oxide fuel cell (SOFC) devices [3–5]. Furthermore, ceramic materials play an important role in development of some modern energy technology. Ceramic materials can also offer not only an enhancement in both conductivity and durability, but also show a redox stability in harsh conditions [6–9]. Perovskite materials have displayed interesting physical, chemical, mechanical, and electrical properties related to their crystal structure and ordering [10–12]. Meanwhile, substitution of lanthanides Ln (La, Sm, Nd, Pr, etc.) in perovskite structures has shown a superior performance in SOFCs utilizations [13,14]. Apparently, these are giving the possibility to use newly synthesised materials as a part of the SOFC component. Furthermore, thermal and electrical properties are greatly dependent on the microstructure and phase stability of the material. One of the interesting materials for these applications is doped $SmFeO_3$. Therefore, investigation of the structure of Zr-doped $SmFeO_3$ [15–17] can measure the possibility of their application in energy devices with high stability based on the presence of Zr^{4+} in the structure.

It was already reported that samarium oxide (Sm_2O_3) is a good catalyst with high activation energy [18–20]. It was also confirmed that doping with Ni^{3+} and Ce^{3+} to $SmFeO_3$ resulted in a noticeable stability [21] with structure having orthorhombic symmetry with *Pnma* or *Pbnm* space groups [15,16,22,23]. The analyses of Sm^{3+} doped materials [10] also showed that the conver-

*Corresponding authors: tel: +6737219025,
e-mail: *abdalla.m.a1984@gmail.com* (Abdalla M. Abdalla)
shahzad_baec@yahoo.com (Shahzad Hossain)
abul.azad@ubd.edu.bn (Abul K. Azad)

sion of the Sm^{3+} to Sm^{2+} species can happen at the same time as the oxidation. So these modifications may justify more research on the use of samarium based materials as possible electrode in SOFC devices. $LnFeO_3$ perovskites showed mixed ionic conductivity when applied as electrode materials (especially as cathodes). They exhibit high amount of oxygen vacancies and a good surface kinetics as well [24–28]. Moreover, Sm doped Fe_2O_3 has proven to have a stable, good catalytic activity which can enhance performance as a gas sensor material in reduced atmosphere [21]. This easily leads to high electrical conductivity of the perovskite because of high electrochemical performance. Further on, tolerancy to the carbon coking and H_2S poisoning depends on the B-site cations [29]. Zn and Zr doped Fe_2O_3 have also been investigated showing a superior performance in structural, magnetic and photocatalytic properties [30–32]. High electrochemical performance of Zn doped materials was achieved in nanosphere Fe_2O_3 [31]. Meanwhile, Zr has shown a high stability and better performance when doped to Fe_2O_3 nanostructure array in photo-electrochemical H_2 production [32].

In this study we have investigated structure of a series of new compounds $Sm_{1-x}Fe_{1-3x}Zr_{3x}O_3$ (x = 0.0, 0.01, 0.02, 0.033, 0.05, 0.1 and 0.15) synthesised by solid state reaction method in order to improve their electrical properties. The doping of the well-known ABO_3 perovskite structure with Zr^{4+} was on the B site (Fe^{3+}). Hence, high stability of these materials made it very suitable for the catalytic activity of the perovskites [33].

II. Experimental procedure

2.1. Sample preparation

New $Sm_{1-x}Fe_{1-3x}Zr_{3x}O_3$ (x = 0.0, 0.01, 0.02, 0.033, 0.05, 0.1 and 0.15) compounds were synthesized by the solid state reaction method in air. Initially, the stoichiometric amounts of high purity (>99.9%) precursors, Sm_2O_3, Fe_2O_3 and ZrO_2, were mixed together. To eliminate the effect of hydration and remove residues, chemicals were heated in air at 300 °C for 2 h inside a muffle furnace. After that, 5 g of each composition was well mixed with ethanol in an agate mortar with pestle. The ethanol was evaporated at RT in a fume cupboard. Then the obtained powders were dried in the oven at 80 °C for 24 hours. The obtained powders were heated in air atmosphere at 900 °C for 10 hours. The collected powders were sonicated for 30 min to get well and homogeneous mixture and the materials were ball milled for 2 h. Afterwords, the obtained dry powder and binder (Decoflux™) were mixed together and pressed into pellets using a hydraulic press (pressure was 2 tonnes) and die with diameter of 15 mm. The pressed pellets (15 mm in diameter and 2 mm thickness) were fired at 1300 °C for 12 hours in the first sintering step. The XRD analysis confirmed that the pure phase was not obtained. Because of that, the pellets were re-ground with ethanol in a mortar with pestle and re-pelletized for the final sintering at temperature of 1500 °C for 15 hours with a heating and cooling rate of 5 °C/min.

2.2. Characterization

The initial structural characterization of the SFZO samples was performed by XRD (Shimadzu-7000, Shimadzu, Japan) using CuKα radiation (λ = 1.5406 Å) in the 2θ range from 10° to 90° with a scan step of 0.01°/s. The procedure utilized here was to identify the structure based on indexing and find the lattice parameters using the WINXPOW [34] and SPuDS [35], respectively. FullProf software [36] was used to perform the Rietveld refinement of the XRD data. The least-square refinement was converged with the minimum goodness of fit (χ^2) and agreed with the literature data [16,17,21]. Scanning electron microscope (SEM-JSM-7610F) was used to investigate microstructure of the sintered samples.

DC electrical conductivity was measured using a four probes DC conductivity jig - SS scientific laboratory supplies at the temperatures up to 850 °C in air atmosphere.

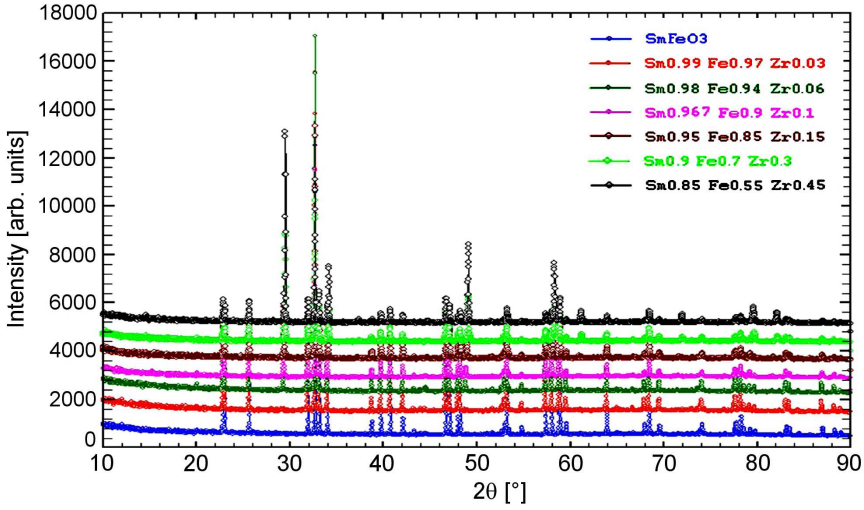

Figure 1. XRD patterns of $Sm_{1-x}Fe_{1-3x}Zr_{3x}O_3$ ($0 \geq x \geq 0.15$) sintered at 1500 °C

Table 1. Atomic positions (*x*, *y*, *z*, O1, O2) of all atoms in the compounds

Chemical compound	Sm (x, y, z)	Fe (x, y, z)	Zr (x, y, z)	O1 (x, y, z)	O2 (x, y, z)
$SmFeO_3$	0.98361, 0.05500, 0.25000	0.50000, 0.00000, 0.00000	—	0.70407, 0.29969, 0.04363	0.08383, 0.46607, 0.25000
$Sm_{0.99}Fe_{0.97}Zr_{0.03}O_3$	0.98361, 0.05500, 0.25000	0.50000, 0.00000, 0.00000	0.50000, 0.00000, 0.00000	0.70407, 0.29969, 0.04363	0.08383, 0.46607, 0.25000
$Sm_{0.98}Fe_{0.94}Zr_{0.06}O_3$	0.98652, 0.05706, 0.25000	0.50000, 0.00000, 0.00000	0.50000, 0.00000, 0.00000	0.70407, 0.29969, 0.04363	0.08383, 0.46607, 0.25000
$Sm_{0.967}Fe_{0.9}Zr_{0.1}O_3$	0.98361, 0.05500, 0.25000	0.50000, 0.00000, 0.00000	0.50000, 0.00000, 0.00000	0.75292, 0.27207, 0.06252	0.10040, 0.49337, 0.25000
$Sm_{0.95}Fe_{0.85}Zr_{0.15}O_3$	0.98874, 0.05500, 0.25000	0.50000, 0.00000, 0.00000	0.50000, 0.00000, 0.00000	0.73360, 0.31732, 0.05914	0.08383, 0.41607, 0.25000
$Sm_{0.9}Fe_{0.7}Zr_{0.3}O_3$	0.98967, 0.05500, 0.25000	0.50000, 0.00000, 0.00000	0.50000, 0.00000, 0.00000	0.70407, 0.32270, 0.04363	0.08383, 0.46607, 0.25000
$Sm_{0.85}Fe_{0.55}Zr_{0.45}O_3$	0.98689, 0.05500, 0.25000	0.50000, 0.00000, 0.00000	0.50000, 0.00000, 0.00000	0.70407, 0.32270, 0.04363	0.08383, 0.46607, 0.25000

Table 2. Cell parameters and *R* factors after the Rietveld refinements of the compositions

Chemical compound	S.G.	*a* [Å]	*b* [Å]	*c* [Å]	R_P	R_{wp}	R_{exp}	R_f	χ^2
$SmFeO_3$	*Pbnm*	5.399369	5.599891	7.708157	3.68	5.08	3.98	11.3	1.63
$Sm_{0.99}Fe_{0.97}Zr_{0.03}O_3$	*Pbnm*	5.399644	5.60576	7.709810	3.15	4.52	3.46	10.70	1.76
$Sm_{0.98}Fe_{0.94}Zr_{0.06}O_3$	*Pbnm*	5.402655	5.604801	7.714882	3.25	4.68	3.42	10.4	1.87
	$Fm\bar{3}m$	5.272561						12.22	
$Sm_{0.967}Fe_{0.9}Zr_{0.1}O_3$	*Pbnm*	5.402901	5.600501	7.713689	3.82	5.08	4.03	10.8	1.60
	$Fm\bar{3}m$	5.268887						8.11	
$Sm_{0.95}Fe_{0.85}Zr_{0.15}O_3$	*Pbnm*	5.402904	5.600665	7.715035	4.27	6.04	4.10	11.4	2.17
	$Fm\bar{3}m$	5.263103						7.92	
$Sm_{0.9}Fe_{0.7}Zr_{0.3}O_3$	*Pbnm*	5.402928	5.601116	7.715492	5.27	7.76	4.57	13.3	2.59
	$Fm\bar{3}m$	5.238837						3.76	
$Sm_{0.85}Fe_{0.55}Zr_{0.45}O_3$	*Pbnm*	5.402953	5.601265	7.715016	5.79	8.77	4.58	12.09	3.67
	$Fm\bar{3}m$	5.244097						2.03	

Table 3. Cell parameters and *R* factors after the Rietveld refinements of the compositions

Chemical compound	Sm	Fe	Zr	O1	O2	ρ_t [g/cm^3]	ρ_b [g/cm^3]	ρ_r [%]
$SmFeO_3$	1.0	1.0	-	2.0	1.0	7.25	6.97	98.19
$Sm_{0.99}Fe_{0.97}Zr_{0.03}O_3$	0.99	0.97	0.03	2.0	1.0	7.29	6.71	92.11
$Sm_{0.98}Fe_{0.94}Zr_{0.06}O_3$	0.92	0.96	0.04	1.95	1.0	7.35	6.69	90.74
	0.06	-	0.02	0.05	-			
$Sm_{0.967}Fe_{0.9}Zr_{0.1}O_3$	0.92	0.89	0.09	2.1	0.89	7.07	5.99	88.49
	0.08	-	0.02	0.05	-			
$Sm_{0.95}Fe_{0.85}Zr_{0.15}O_3$	0.90	0.8	0.15	2.11	0.79	7.19	5.85	87.14
	0.05	-	0.02	0.05				
$Sm_{0.9}Fe_{0.7}Zr_{0.3}O_3$	0.87	0.74	0.3	2.0	0.92	7.66	6.35	83.95
	0.03	-	0.02	0.05	-			
$Sm_{0.85}Fe_{0.55}Zr_{0.45}O_3$	0.8	0.6	0.40	1.9	0.86	7.18	6.02	82.87
	0.05	-	0.05	0.05				

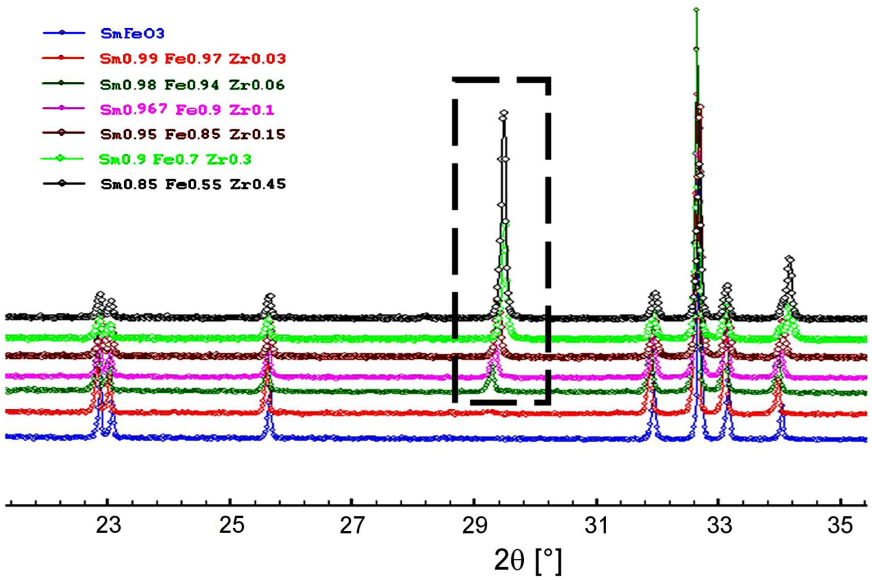

Figure 2. Highlighted XRD peak 011 of the cubic phase of the prepared samples for $x \geq 0.02$

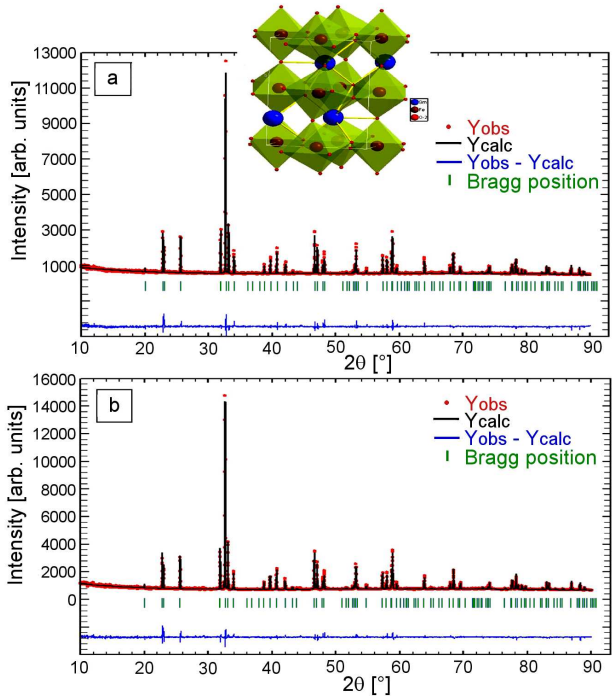

Figure 3. Rietveld refinement and crystal structure of: a) $SmFeO_3$ and b) $Sm_{0.99}Fe_{0.97}Zr_{0.03}O_3$

III. Results and discussion

3.1. Structure determination

The XRD diffraction patterns of $Sm_{1-x}Fe_{1-3x}Zr_{3x}O_3$ (x = 0.0, 0.01, 0.02, 0.033, 0.05, 0.10 and 0.15) pellets sintered at 1500 °C are presented in Fig. 1. It is obvious that the single phase materials were obtained for x = 0.0 and 0.01, whereas the secondary phase appeared for $x \geq$ 0.02. The selected 2θ regions, showing the appearance and growth of the secondary phase, are given in Fig. 2.

The Rietveld analyses of the XRD data (Figs. 3 and 4) give the correct atomic positions, space group and cell parameters. The analyses confirmed that the materials for x = 0.0 and 0.01 crystallize in the single phase orthorhombic structure with the space group *Pbnm*. A small amount of the second phase with cubic symmetry and space group $Fm\bar{3}m$ was found to be coexisting in the SFZO ceramics with x = 0.02, 0.033, 0.05, 0.1 and 0.15. The structure with higher Zr-content ($x \geq 0.02$) was found to be two-phase system with orthorhombic and cubic symmetry, characterized with the splitting of some major peaks. The atomic positions of the investigated samples are illustrated in Table 1. The cell parameters after the Rietveld refinement of the sintered SFZO ceramics are given in Table 2 and the atomic occupancies, bulk and theoretical densities of the SFO and SFZO are shown in Table 3. It was observed that the lattice parameters of the perovskite structure increase with Zr doping. This slightly increase is due to the differences in ionic radii of Zr^{4+} and Fe^{3+} (radius of Zr^{4+} is higher than that of Fe^{3+}) and the Zr^{4+} occupies the B-site. However, for the SFZO samples with $x \geq 0.02$ the lattice parameter of the fluorite structure has decreasing trend, due to the oxidation state of iron ion.

3.2. Microstructural study

The microstructure of the materials was examined by using SEM (Fig. 5). It is obvious that addition of Zr increases level of porosity in the sintered samples. Hence, it is recommended that this material can be used for oxygen sensor and SOFCs electrode applications [37–41] depending on their electrochemical and electrical conductivity with a good chemical and thermal stability. Thus, based on the previous results, i.e. $SmFeO_3$ with another dopant like Ce [20,21], it is possible to obtain high performance material for electrode application in fuel cell systems, with fast oxygen transport [42,43] as well as high electrocatalitic performances.

From the density calculations, from both experimental and theoretical [44], it is clear that there is a very

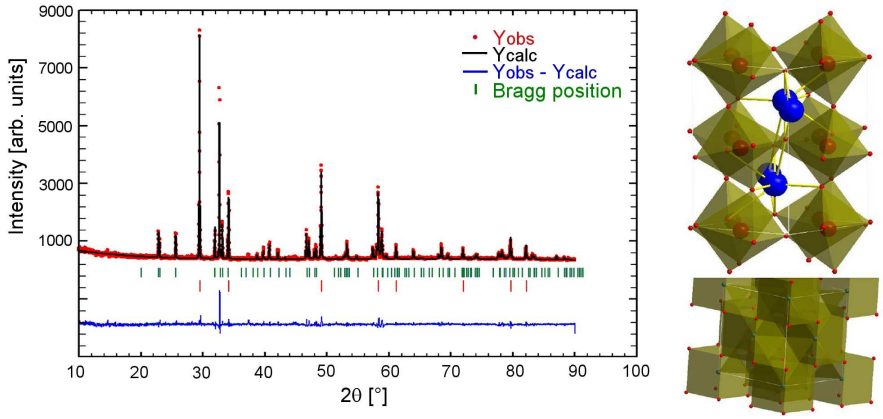

Figure 4. Rietveld refinement (a) and crystal structure (b) of two-phase ceramics ($Sm_{0.85}Fe_{0.55}Zr_{0.45}O_3$)

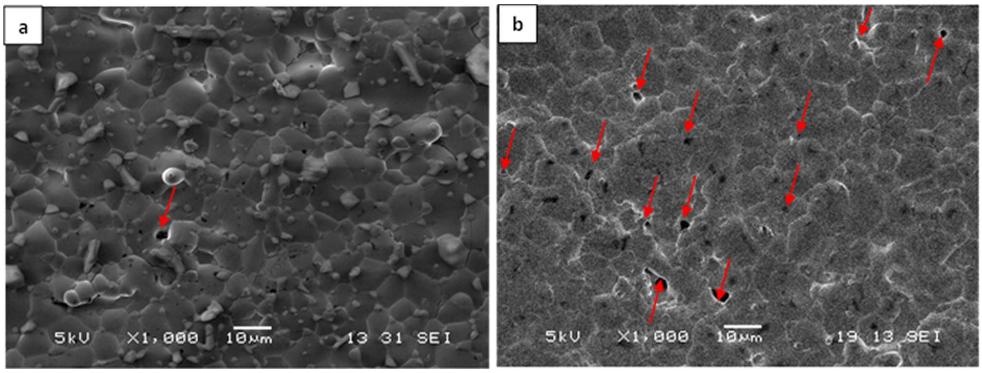

Figure 5. SEM micrographs of the samples: a) $SmFeO_3$ and b) $Sm_{0.99}Fe_{0.97}Zr_{0.03}O_3$ sintered at 1500 °C

strong relation between the porosity and amount of Zr added to $SmFeO_3$. As shown in Table 3 in the samples with higher amount of Zr the lower density was obtained. Thus, the pure $SmFeO_3$ has relative density of 98.2 %TD and relative density of $Sm_{0.85}Fe_{0.55}Zr_{0.45}O_3$ is 82.9 %TD. This significant decrease in density resulting from Zr addition was confirmed by SEM analyses.

Moreover, the obtained microstructure gives an excellent stability and reversibility of oxygen storage-related process [45,47]. Accordingly, it is very easy to predict the occurrence of high transportation in SFZO oxides because of the porosity increases without adding any pore former [41,43].

3.3. Electrical conductivity

Three sintered samples: $SmFeO_3$, $Sm_{0.99}Fe_{0.97}Zr_{0.03}O_3$ (with single phase structures) and $Sm_{0.98}Fe_{0.94}Zr_{0.06}O_3$ (with two-phase structure) were selected to investigate the electrical properties in terms of DC conductivity in air atmosphere. Four thin gold wires were attached on different positions on the sample surface (Fig. 6) with the gold paste and heated at 700 °C for 1 hour with 2 °C/min heating and cooling rate. Afterwards, the bar was fixed on the measuring jig and the probes of the jig were attached to the four terminals of the sample. Then the set up was inserted into the chamber and tested at the temperature up to 850 °Cin air with 4 °C/min heating and cooling rate.

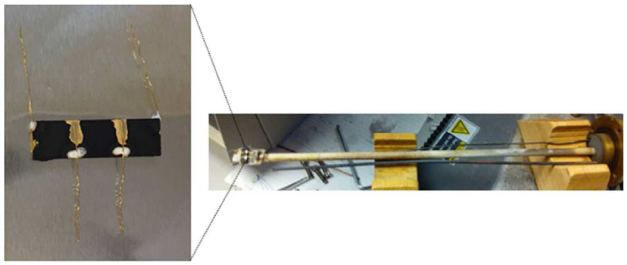

Figure 6. Enlarged view of the sintered bar attached with gold wires and fixed in the test jig position

Figure 7 shows the conductivity results of the three tested samples. The conductivity was calculated by using the Uhlir equation [47]:

$$\sigma = \frac{d}{R \cdot t \cdot L_{av}} \tag{1}$$

where d is the spacing between two attached wires, t is the bar thickness and L_{av} is the effective length during the measurements. The continuous increase of conductivity with temperature is obvious in all three samples (Fig. 7). The highest electrical conductivity at 850 °C of 0.045 S/cm has the sample $Sm_{0.99}Fe_{0.97}Zr_{0.03}O_3$, considerably higher in comparison to the value of 0.007 S/cm for the pure $SmFeO_3$. The sample $Sm_{0.98}Fe_{0.94}Zr_{0.06}O_3$, which contains a small amount of secondary phase, still has relatively high electrical conductivity of 0.025 S/cm at 850 °C in air (shown in Fig. 7c).

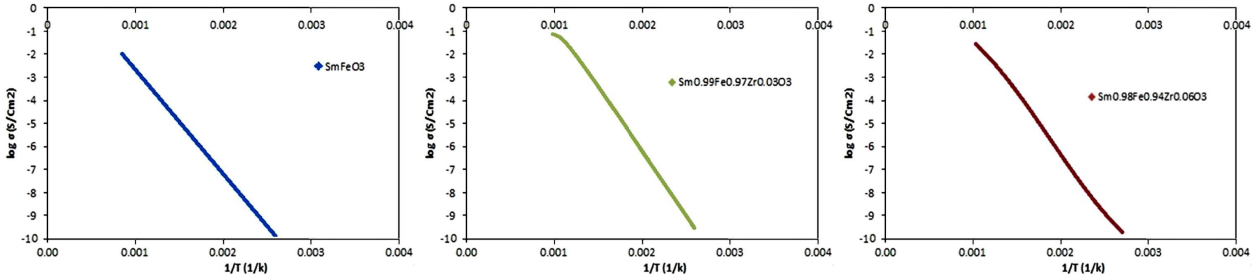

Figure 7. Arrhenius plots of conductivity of: a) $SmFeO_3$, b) $Sm_{0.99}Fe_{0.97}Zr_{0.03}O_3$ and c) $Sm_{0.98}Fe_{0.94}Zr_{0.06}O_3$

IV. Conclusions

Standard solid state reaction method was used to synthesize a series of new materials $Sm_{1-x}Fe_{1-3x}Zr_{3x}O_3$ (x = 0.0, 0.01, 0.02, 0.033, 0.05, 0.10, and 0.15) successfully and investigate the structural, microstructural and electrical properties. The Rietveld refinement of XRD data indicated that these samples possess an orthorhombic single phase crystal structure for x = 0.0 and 0.01 in the *Pbnm* space group. However, slightly higher Zr-doped materials ($\geq$ 0.02) have a small amount of cubic fluorite phase which was refined together with the main phase to get accurate structural information in $Sm_{1-x}Fe_{1-3x}Zr_{3x}O_3$ at $x \geq 0.02$. Those materials have shown two-phase structures of orthorhombic (perovskite) and cubic (fluorite) type. Microstructures of the single phase materials demonstrated a slight increase in porosity with Zr doping with almost the same particle size of 20 μm (both in SFO and SFZ oxides). The increase of Zr dopant resulted in an increase in electrical conductivity compared to the un-doped $SmFeO_3$ material. Based on the obtained DC conductivity results, Zr doped $SmFeO_3$ showed a noticeable improvement which indicates their ability to be applied in various applications, such as gas sensors and SOFC electrodes.

Acknowledgement: The authors, AMA and SH are thankful to the University Brunei Darussalam (Graduate studies office) for providing them the funding as GRS (Graduate Research Scholarship) to perform this research.

References

1. C.C. Fischer, K.J. Tibbetts, D. Morgan, G. Ceder, "Predicting crystal structure by merging data mining with quantum mechanics", *Nature Mater.*, **5** (2006) 641–646.
2. G. Birkhoff, J. Von Neumann, "The logic of quantum mechanics", *Ann. Math.*, **37** [4] (1936) 823–843.
3. J. Ayache, L. Beaunier, J. Boumendil, G. Ehret, D. Laub, *Sample Preparation Handbook for Transmission Electron Microscopy: Methodology*, Chap. 2. 1st Ed. Springer, New York, 2010.
4. S. Hossain, A.M. Abdalla, S.N. Binti Jamain, J.H. Zaini, A.K. Azad, "A review on proton conducting electrolytes for clean energy and intermediate temperature-solid oxide fuel cells", *Renew. Sust. Energy Rev.*, **79** (2017) 750–764.
5. A.M. Abdalla, S. Hossain, A.T. Azad, P.M. I. Petra, F. Begum, S.G. Eriksson, A.K. Azad, "Nanomaterials for solid oxide fuel cells: A review", *Renew. Sust. Energy Rev.*, **82** (2018) 353–368.
6. J.C. Ruiz-Morales, D. Marrero-López, M. Gálvez-Sánchez, J. Canales-Vázquez, C. Savaniu, S.N. Savvin, "Engineering of materials for solid oxide fuel cells and other energy and environmental applications", *Energy Environ. Sci.*, **3** [11] (2010) 1670–1681.
7. J. Grenier, J. Bassat, F. Mauvy, *Functional Materials for Sustainable Energy Applications*, Woodhead Publishing Limited, 2012.
8. B. Lin, S. Zhang, L. Zhang, L. Bi, H. Ding, X. Liu, J. Gao, G. Meng, "Prontonic ceramic membrane fuel cells with layered $GdBaCo_2O_{5+x}$ cathode prepared by gel-casting and suspension spray", *Power Sources*, **177** (2008) 330–333.
9. S. Kang, P. Heo, Y. Ho, J. Ha, I. Chang, S. Cha, "Low intermediate temperature ceramic fuel cell with Y-doped $BaZrO_3$ electrolyte and thin film Pd anode on porous substrate", *Electrochem. Commun.*, **13** [4] (2011) 374–377.
10. S. Rada, P. Pascuta, M. Rada, E. Culea, "Effects of samarium (III) oxide content on structural investigations of the samarium-vanadate-tellurate glasses and glass ceramics", *J. Non-Cryst. Solids*, **357** [19-20] (2011) 3405–3409.
11. M.V. Sandoval, A. Matta, T. Matencio, R. Zacarias Domingues, G.A. Ludwig, M. De Angelis Korb, C. De Fraga Malfatti, P. Gauthier-Maradei, G.H. Gauthier, "Barium-modified NiO-YSZ/NiO-GDC cermet as new anode material for solid oxide fuel cells (SOFC)", *Solid State Ionics*, **261** (2014) 36–44.
12. A.M. Abdalla, S. Hossain, P.M.I. Petra, C.D. Savaniu, J.T.S. Irvine, A.K. Azad, "Novel layered perovskite $SmBaMn_2O_{5+d}$ for SOFCs anode material", *Mater. Lett.*, **204** (2017) 129–132.
13. A. Orera, P. Slater, "New chemical systems for solid oxide fuel cells", *Chem. Mater.*, **22** [3] (2010) 675–690.
14. S. Chaianansutcharit, K. Hosoi, J. Hyodo, Y. Ju, T. Ishihara, "Ruddlesden popper oxides of $LnSr_3Fe_3O_{10-\delta}$ (Ln = La, Pr, Nd, Sm, Eu, and Gd) as active cathodes for low temperature solid oxide fuel cells", *Mater. Chem. A*, **3** (2015) 12357–12366.
15. S.M. Bukhari, J.B. Giorgi, "Electrical conductivity dependence of Ni doped $Sm_{0.95}Ce_{0.05}FeO_{3-\delta}$ on surface morphology and composition", *Sensors Actuat. B Chem.*, **155** [2] (2011) 524–537.
16. S.M. Bukhari, J.B. Giorgi, "Tuneability of $Sm_{(1-x)}Ce_xFeO_{3\pm\lambda}$ perovskites: Thermal stability and electrical conductivity", *Solid State Ionics*, **180** [2-3] (2009) 198–204.
17. S. Yuvaraj, S. Layek, S.M. Vidyavathy, S. Yuvaraj, D. Meyrick, R.K. Selvan, "Electrical and magnetic properties of spherical $SmFeO_3$ synthesized by aspartic acid assisted

combustion method", *Mater. Res. Bull.*, **72** (2015) 77–82.
18. A.A. Tolstopyatova, Yü Chi-Chüan, L.S. Gorshkova "Catalytic properties of samarium oxide with respect to the dehydrogenation and dehydration of alcohols and the dehydrogenation of tetralin", *Russian. Chem. Bull.*, **13** [1] (1964) 6–9.
19. G.A.M. Hussein, D.J. Buttrey, P. DeSanto Jr., A.A. Abd-Elgaber, H. Roshdy, A.Y.Z. Myhoub, "Formation and characterization of samarium oxide generated from different precursors", *Thermochim. Acta*, **402** [1-2] (2003) 27–36.
20. W. Liu, Y. Liu, B. Li, T. D. Sparks, X. Wei, W. Pan. "Ceria (Sm^{3+},Nd^{3+})/carbonates composite electrolytes with high electrical conductivity at low temperature", *Compos. Sci. Technol.*, **70** [1] (2010) 181–185.
21. S.M. Bukhari, J.B. Giorgi, "Surface and redox chemistry of $Sm_{0.95}Ce_{0.05}Fe_{1-x}Ni_xO_{3-\delta}$ perovskites", *Solid State Ionics*, **194** (2011) 33–40.
22. H. Xu, X. Hu, L. Zhang, "Generalized low-temperature synthesis of nanocrystalline rare-earth orthoferrites $LnFeO_3$ (Ln = La, Pr, Nd, Sm, Eu, Gd)", *Crystal Growth Design*, **8** [7] (2008) 2061–2065.
23. W. Fan, Z. Sun, J. Wang, J. Zhou, K. Wu, Y. Cheng, "A new family of Ce-doped $SmFeO_3$ perovskite for application in symmetrical solid oxide fuel cells", *J. Power Sources*, **312** (2016) 223–233.
24. A.E. Giannakas, A.A. Leontiou, A.K. Ladavos, P.J. Pomonis, "Characterization and catalytic investigation of NO + CO reaction on perovskites of the general formula $LaxM_{1-x}FeO_3$ (M = Sr and/or Ce) prepared via a reverse micelles microemulsion route", *Appl. Catalysis A: General*, **309** (2006) 254–262.
25. T. Ishihara, H. Furutani, M. Honda, T. Yamada, T. Shibayama, T. Akbay, N. Sakai, H.Yokokawa, Y. Takita, "Improved oxide ion conductivity in $La_{0.8}Sr_{0.2}Ga_{0.8}Mg_{0.2}O_3$ by doping Co", *Chem. Mater.*, **11** (1999) 2081–2088.
26. T. Ishihara, T. Yamada, H. Arikawa, H. Nishiguchi, Y. Takita "Mixed electronic-oxide ionic conductivity and oxygen permeating property of Fe-, Co- or Ni-doped $LaGaO_3$ perovskite oxide", *Solid State Ionics*, **135** (2000) 631–636.
27. V.V. Kharton, A.P. Viskup, E.N. Naumovich, N.M. Lapchuk, "Mixed electronic and ionic conductivity of $LaCo(M)O_3$ (M = Ga, Cr, Fe or Ni): I. Oxygen transport in perovskites $LaCoO_3$-$LaGaO_3$", *Solid State Ionics*, **104** (1997) 67–78.
28. M. Mori, Y. Iwamoto, M. Asamoto, Y. Itagaki, H. Yahiro, Y. Sadaoka, S. Takase, Y. Shimizu, M. Yuasa, K. Shimanoe, H. Kusaba, Y. Teraoka, "Effect of preparation routes on the catalytic activity over $SmFeO_3$ oxide", *Catal. Today*, **139** (2008) 125–129.
29. S.V Trukhanov, A.V Trukhanov, H. Szymczak, R. Szymczak, M. Baran, "Thermal stability of A-site ordered $PrBaMn_2O_6$ manganites", *J. Phys. Chem. Solids*, **67** (2006) 675–681.
30. Z.H. Hua, S.Z. Li, Z.D. Han, D.H. Wang ,M. Lu, W. Zhong, B.X. Gu, Y.W. Du, "The effect of La-Zn substitution on the microstructure and magnetic properties of barium ferrites", *Mater. Sci. Eng. A*, **448** (2007) 326–329.
31. X. Qi, G. She, M. Wang, L. Mu, W. Shi "Electrochemical synthesis of p-type Zn-doped α-Fe_2O_3 nanotube arrays for photoelectrochemical water splitting", *Chem. Commun.*, **49** (2013) 5742–5744.
32. V. Yadav, S. Tyagi, D. Pundhir, S.K. Gupta, "Comparative study of nanostructured Zr-Fe_2O_3 and CNT modified Zr-Fe_2O_3 thin films for photo electrochemical generation of hydrogen", *J. Nanoanalysis*, **1** [3] (2014) 125–128
33. L. Hui, M. Futai, M. Zuzhu, L. Haiyang, X. Yabo "Study of the reactivity of surface oxygen species on $SmMnO_3$ and $SmFeO_3$ catalysts", *J. Alloys Compd.*, **193** (1993) 68–69.
34. A. Yaqub, C. Savaniu, N.K. Janjua, J.T.S. Irvine, "Preparation via a solution method of $La_{0.2}Sr_{0.25}Ca_{0.45}TiO_3$ and its characterization for anode supported solid oxide fuel cells", *J. Mater. Chem. A*, **1** (2013) 14189–14197.
35. M.W. Lufaso, P.M. Woodward, "Prediction of the crystal structures of perovskites using the software program SPuDS", *Acta Crystallogr. B*, **57** (2001) 725–738.
36. J. Rodríguez-Carvajal, "Recent advances in magnetic structure determination by neutron powder diffraction", *Physica B*, **192** (1993) 55–69.
37. I. Ahmed, M. Karlsson, S. Eriksson, E. Ahlberg, C.S. Knee, "Crystal structure and proton conductivity of $BaZr_{0.9}Sc_{0.1}O_{3-d}$", *J. Am. Ceram. Soc.*, **91** [9] (2008) 3039–3044.
38. M. Mori, Y. Iwamoto, M. Asamoto, Y. Itagaki, H. Yahiro, Y. Sadaoka, S. Takase, Y. Shimizu, M. Yuasa, K. Shimanoe, H. Kusaba, Y. Teraoka, "Effect of preparation routes on the catalytic activity over $SmFeO_3$ oxide", *Catal. Today*, **139** (2008) 125–129
39. W. Fan, Z. Sun, J. Wang, J. Zhou, K. Wu, Y. Cheng, "A new family of Ce-doped $SmFeO_3$ perovskite for application in symmetrical solid oxide fuel cells", *J. Power Sources*, **312** (2016) 223–233.
40. X. Wang, J. Yu, X. Yan, Y. Long, K. Ruan, X. Li, "Magnetization and low temperature heat capacity of $SmFeO_3$ single crystal", *J. Magn. Magn. Mater.*, **443** (2017) 104–106.
41. C.W. Tanner, K.-Z. Fung, A.V. Virkar, "The effect of porous composite electrode structure on solid oxide fuel cell performance", *Electrochem. Soc.*, **144** [1] (1997) 21–30.
42. F. Dong, M. Ni, Y. Chen, D. Chen, M. O. Tadé, Z. Shao, "Structural and oxygen-transport studies of double perovskites $PrBa_{1-x}Co_2O_{5+\delta}$ (x = 0.00, 0.05, and 0.10) toward their application as superior oxygen reduction electrodes", *J. Mater. Chem. A*, **2** (2014) 20520–20529.
43. X.M. Ge, S.H. Chan, Q.L. Liu, Q. Sun, "Solid oxide fuel cell anode materials for direct hydrocarbon utilization", *Adv. Energy Mater.*, **2** [10] (2012) 1156–1181.
44. A.M. Abdalla, S. Hossain, J. Zhou, Pg. M.I. Petra, S. Erikson, C.D. Savaniuc, J.T.S. Irvine, A.K. Azad "$NdBaMn_2O_{5+\delta}$ layered perovskite as an active cathode material for solid oxide fuel cells", *Ceram. Int.*, **43** (2017) 15932–15938.
45. S.V. Trukhanov, A.V. Trukhanov, H. Szymczak, R. Szymczak, M. Baran, "Thermal stability of A-site ordered $PrBaMn_2O_6$ manganites", *Phys. Chem. Solids*, **67** (2006) 675–681.
46. X. Huang, C. Ni, G. Zhao, J.T.S. Irvine, "Oxygen storage capacity and thermal stability of $CuMnO_2$-CeO_2 composite system", *Mater. Chem. A*, **2** (2015) 12958–12964.
47. A. Uhlir, "The potentials of infinite systems of sources and numerical solutions of problems in semiconductor engineering", *Bell Syst. Techn. J.*, **34** (1955) 105–128.